Check for updates

Received: 1 April 2026 | Revised: 1 June 2026 | Accepted: 5 June 2026

DOI: 10.1002/ctd2.70160

CLINICAL AND TRANSLATIONAL DISCOVERY Open Access WILEY

RESEARCH ARTICLE

TGF-β1-driven epithelial–mesenchymal transition mediates the fibrotic process in IgG4-related disease

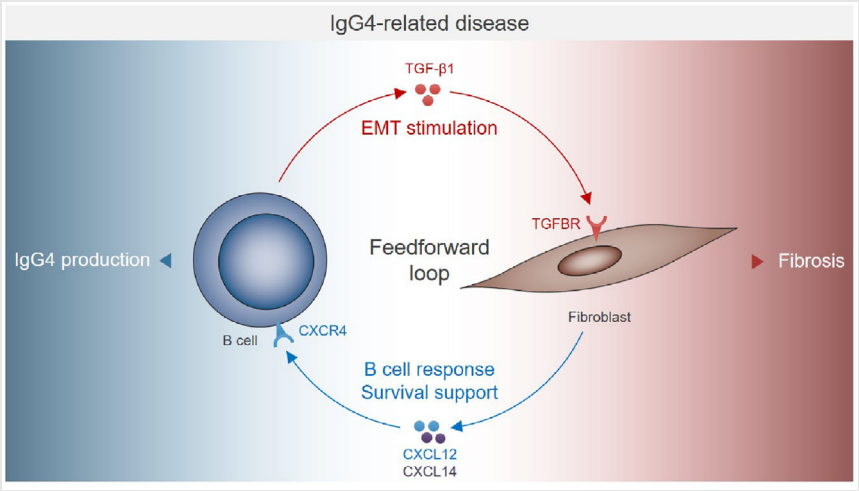
In-Woon Baek[1] | **Kyung-Su Park**[2] | **Ki-Jo Kim**[2]

[1]Division of Rheumatology, Department of Internal Medicine, Ewha Womans University, College of Medicine, Seoul, Republic of Korea

[2]Division of Rheumatology, Department of Internal Medicine, St. Vincent's Hospital, College of Medicine, The Catholic University of Korea, Seoul, Republic of Korea

Correspondence
Ki-Jo Kim, St. Vincent's Hospital, 93 Jungbu-daero, Paldal-gu, Suwon 16247, Republic of Korea.
Email: md21c@catholic.ac.kr

Graphical Abstract



In IgG4-related disease, the epithelial-to-mesenchymal transition of fibroblasts was predominantly driven by transforming growth factor-β1 secreted from $CD19^+$ B cells. Reciprocally, fibroblasts facilitated $CD19^+$ B-cell survival and activation through CXCL14–CXCR4 and CXCL12–CXCR4 signalling axes, thereby promoting B-cell responses and subsequent antibody production.

Received: 1 April 2026 | Revised: 1 June 2026 | Accepted: 5 June 2026

DOI: 10.1002/ctd2.70160

RESEARCH ARTICLE

CLINICAL AND TRANSLATIONAL DISCOVERY Open Access

WILEY

TGF-β1-driven epithelial–mesenchymal transition mediates the fibrotic process in IgG4-related disease

In-Woon Baek[1] | **Kyung-Su Park**[2] | **Ki-Jo Kim**[2]

[1]Division of Rheumatology, Department of Internal Medicine, Ewha Womans University, College of Medicine, Seoul, Republic of Korea

[2]Division of Rheumatology, Department of Internal Medicine, St. Vincent's Hospital, College of Medicine, The Catholic University of Korea, Seoul, Republic of Korea

Correspondence
Ki-Jo Kim, St. Vincent's Hospital, 93 Jungbu-daero, Paldal-gu, Suwon 16247, Republic of Korea.
Email: md21c@catholic.ac.kr

Abstract

Background: Major challenges exist in understanding the pathogenic mechanisms and developing systemic therapeutic strategies for IgG4-related disease (IgG4-RD) due to its rarity, unique clinical manifestations and inconsistent response to specific treatments. To overcome these limitations, comprehensive analysis of gene expression profiles may serve as a crucial stepping stone.

Methods: A salivary gland transcriptomic dataset encompassing both bulk tissue and single-cell levels was obtained. Cellular and molecular features were identified by analysing differentially expressed genes and performing functional enrichment analyses. Gene regulatory and cell–cell communication analyses were also conducted.

Results: The most enriched processes were the epithelial–mesenchymal transition (EMT) and extracellular matrix organisation. EMT, which was weighted towards a mesenchymal signature, was closely associated with myofibroblasts, extracellular matrix organisation and the transforming growth factor-β (TGF-β) signalling pathway. Fibroblasts were the primary cell subset enriched for in the EMT signature. Additionally, $CD19^+$ B cells, cytotoxic T cells and regulatory T cells were the main sources of TGF-β1. In the analysis of B cell–fibroblast communication, EMT of fibroblasts was found to be activated primarily by TGF-β1 secreted from $CD19^+$ B cells. Reciprocally, fibroblasts supported $CD19^+$ B cells via CXCL14–CXCR4 and CXCL12–CXCR4 interactions.

Conclusions: Our findings suggest a pivotal role for TGF-β1-mediated EMT in the pathogenesis of fibrosis associated with IgG4-RD, with $CD19^+$ B cells identified as a significant source of TGF-β1. This evidence substantiates the rationale for B-cell-depletion therapy as a promising therapeutic strategy for this condition.

KEYWORDS
B cells, epithelial–mesenchymal transition, fibroblasts, IgG4-related disease, TGF-β

This is an open access article under the terms of the Creative Commons Attribution License, which permits use, distribution and reproduction in any medium, provided the original work is properly cited.
© 2026 The Author(s). *Clinical and Translational Discovery* published by John Wiley & Sons Australia, Ltd on behalf of Shanghai Institute of Clinical Bioinformatics.

27680622, 2026, 3, Downloaded from https://onlinelibrary.wiley.com/doi/10.1002/ctd2.70160 by Ewha Womans University Library, Wiley Online Library on [30/09/2026]. See the Terms and Conditions (https://onlinelibrary.wiley.com/terms-and-conditions) on Wiley Online Library for rules of use; OA articles are governed by the applicable Creative Commons License

1 | INTRODUCTION

IgG4-related disease (IgG4-RD) is a rare fibro-inflammatory disorder characterised by tumefactive lesions, storiform fibrosis and polyclonal IgG4-positive plasma cell-enriched infiltrate, and can affect various internal organs including major salivary glands, lacrimal gland, orbits, pancreas, bile ducts, retroperitoneum, lungs, kidneys, aorta, pachymeninges and thyroid gland.[1–4] IgG4-RD is a chronic and relapsing condition and uncontrolled disease flares may lead to progressive organ dysfunction and failure.[1,5]

The immunopathogenesis of IgG4-RD includes oligoclonal expansions of autoreactive B cells in germinal centers and subsequent elevation of serum IgG4 levels, in addition to complex and multifaceted interactions between B-cell subsets, various $CD4^+$ and $CD8^+$ T lymphocytes, macrophages and fibroblasts that drive tissue injury and fibrosis within affected tissues.[4] Cytokines such as transforming growth factor-β (TGF-β), platelet-derived growth factor-β (PDGF-β), interferon-γ (IFN-γ) and interleukin (IL)-1β and IL-10 play key roles in driving profibrotic activation of fibroblasts.[4] In particular, B lymphocytes contribute directly to tissue fibrosis and extracellular matrix remodelling by producing PDGF-β and lysyl oxidase homologue 2 (LOXL2)[6]; the efficacy of B-cell-depletion therapy using rituximab or inebilizumab in IgG4-RD strongly supports the significant role of B cells in the pathogenesis of IgG4-RD.[5,7,8] However, questions about the long-term safety, maintenance therapy formulation and comparative efficacy of rituximab or inebilizumab compared to other B-cell-targeting therapies remain to be addressed.[4,9]

The coexistence of fibrotic and chronic inflammatory components, while not diagnostic, is a prerequisite histological feature of IgG4-RD.[1,4] Coupling of fibrotic processes to preceding aberrant immunological responses or concomitant inflammation can vary, being either partially coupled or uncoupled based on the underlying disease or pathological environment.[10] Fibrosis in some fibrotic diseases such as systemic sclerosis and idiopathic pulmonary fibrosis is not fully controlled by glucocorticoids or immunosuppressive therapy.[11,12] Further understanding of context-dependent mechanisms of fibrosis and additional treatment strategies to interfere with the fibrotic process are required to effectively suppress on-going fibrosis.

Tissue transcriptome profiling, encompassing both bulk and single-cell approaches, is an ideal tool with which to delineate pathobiological landscapes and elucidate aberrant cellular and molecular signatures associated with disease. For this study, we imported transcriptomic data from salivary glands of patients with IgG4-RD affecting the major salivary glands. We employed advanced bioinformatic tools to analyse the cellular and molecular characteristics of the inflammatory and fibrotic processes. We focused on key pathogenic mechanisms, and identified molecules associated with these processes. Finally, we elucidated the core pathology of tissue fibrosis and the pivotal role of B cells in this process, highlighting the therapeutic potential of targeting B cells in IgG4-RD.

2 | METHODS

2.1 | Data collection

We imported blood transcriptomic datasets from Gene Expression Omnibus: GSE40568 for IgG4-RD,[13] GSE40611 for Sjögren's disease (SjD) and non-SjD sicca syndrome,[14] and GSE3526 and GSE7307 for healthy controls. Although SjD and non-SjD sicca syndrome share overlapping clinical manifestations with IgG4-RD, they represent distinct disease entities requiring accurate differential diagnosis; accordingly, both were included as disease controls in the present analysis. In total, salivary gland samples were collected from five patients with IgG4-RD, 22 patients with SjD, 14 patients with non-SjD sicca syndrome and 30 healthy controls (Tables S1–S3). A single-cell RNA sequencing (scRNA-seq) dataset of salivary glands from four patients with IgG4-RD was retrieved from GSE242778.[15]

2.2 | Preprocessing of gene expression data

All analyses were performed using R (version 4.5.1, The R Project for Statistical Computing, www.r-project.org). For Affymetrix microarray data, the robust multi-array average (RMA) method was employed for background correction, normalisation and probe set summarisation.[16] The RMA method incorporates quantile normalisation, which equalises data distributions across arrays to ensure comparability among samples. We specifically used the affy package in R for this one-channel Affymetrix array processing. Residual technical batch effects, which arise from the integration of multiple heterogeneous datasets, were corrected using the ComBat method.[17] This method uses either parametric or non-parametric empirical Bayes frameworks to adjust the data for batch effects. We selected a combination of quantile normalisation and the ComBat function for quality control due to its demonstrated superior performance compared to other methods.[18,19] Principal component analysis was used to assess dataset

27680622, 2026, 3, Downloaded from https://onlinelibrary.wiley.com/doi/10.1002/ctd2.70160 by Ewha Womans University Library, Wiley Online Library on [30/09/2026]. See the Terms and Conditions (https://onlinelibrary.wiley.com/terms-and-conditions) on Wiley Online Library for rules of use; OA articles are governed by the applicable Creative Commons License

quality and distribution bias. After this preprocessing, systematic and dataset-specific biases were significantly reduced compared with the data before normalisation and batch correction (Figure S1).

2.3 | Filtration of differentially expressed genes

Differentially expressed genes (DEGs) were identified using the significance analysis of microarray algorithm, which made it possible to perform one and two class analyses using either a modified *t*-statistic or a (standardised) Wilcoxon rank statistic, in addition to a multiclass analysis using a modified *F*-statistic.[20] DEGs were defined as those with a false discovery rate (FDR) of less than 0.05 and an absolute fold change greater than 1.5.

2.4 | Prioritisation of disease-associated genes

To further prioritise disease-associated genes within the human interactome, we employed the TOP–down Attachment of Seeds (TOPAS) algorithm.[21] This iterative approach connects the largest number of seed nodes in a top–down manner. It achieves this by identifying 'connector' nodes that ensure the highest flow of a random walk with restart in a functional association network.

2.5 | Gene-set and cell-type enrichment analyses

A functional enrichment analysis of upregulated DEGs was conducted using Enrichr software, which employs adjusted *p*-values, odds ratios and combined scores as featured enrichment indices.[22] Gene-set enrichment analysis (GSEA) was used to identify a group of genes in a specified list of genes overrepresented compared with a background set of genes.[23] The normalised enrichment score (NES) was used to compare analysis results across gene sets by accounting for variations in gene set size and correlations between the sets and the expression dataset. The preranked GSEA was run using the classic enrichment statistic with 1000 permutations. Gene-set information about signalling pathways and biological processes (BP) was obtained from the Kyoto Encyclopedia of Genes and Genomes, Gene Ontology (GO), Reactome database and Molecular Signatures Database (MSigDB).[24–27] Single-sample enrichment scores for the gene sets were estimated by gene-set variation analysis (GSVA) using the 'gsva' function from the R package GSVA.[28] To deconvolute cellular composition from the tissue sample, we used a digital sorting algorithm that deconvolves the expression profiles of a tissue into the component profiles of each cell type using a set of marker genes that are highly expressed in each cell type.[29] Information about all gene sets used in this study is provided in the Supporting Information.

2.6 | Epithelial–mesenchymal transition score

Signature genes for the generic epithelial–mesenchymal transition (EMT), as well as epithelial and mesenchymal signatures were imported from the MSigDB Hallmark collection and a previous study by Panchy et al.[27,30] Generic EMT, epithelial and mesenchymal scores were then calculated using the AUCell algorithm, in accordance with the methods of previous studies.[30,31]

2.7 | Tumour microenvironment score

Tumour microenvironment score was calculating using the Estimation of Stromal and Immune cells in Malignant Tumour tissues using Expression data (ESTIMATE) algorithm,[32] which includes two gene signatures: (1) a 'stromal signature' that was designed to capture the presence of stroma in tumour tissue, and (2) an 'immune signature' that indicates the infiltration of immune cells in tumour tissue.

2.8 | Human protein–protein interaction network

A human protein–protein interaction (PPI) network was constructed using the FunCoup database,[33] which provide a comprehensive view of the functional coupling interactome. Nodes and edges represent proteins and their functional or physical interactions, respectively. The human network comprises 14 739 nodes and 1 746 571 edges.

2.9 | Single-cell RNA sequencing data analysis

scRNA-seq data of salivary gland tissue from patients with IgG4-RD was retrieved from GSE242778.[15] In more detail, scRNA-seq data of 36 601 single cells isolated from the salivary glands of four patients with IgG4-RD were processed using the Seurat package according to the standard protocol.[34] Clustered cell types were annotated using singleR and the CellTypist toolkits.[35,36]

27680622, 2026, 3, Downloaded from https://onlinelibrary.wiley.com/doi/10.1002/ctd2.70160 by Ewha Womans University Library, Wiley Online Library on [30/09/2026]. See the Terms and Conditions (https://onlinelibrary.wiley.com/terms-and-conditions) on Wiley Online Library for rules of use; OA articles are governed by the applicable Creative Commons License

2.10 | Gene regulatory network analysis

We employed the Single-Cell Regulatory Network Inference and Clustering (SCENIC) approach with default parameters to identify activated regulons and their activities within each cell subtype.[31] The process involves three main steps. (1) Gene regulatory network (GRN) inference: co-expressed modules are first inferred using a regression-per-target approach (GRNBoost2). (2) Module pruning: indirect targets are then pruned from these modules through cis-regulatory motif discovery (cisTarget). (3) Regulon activity quantification: the activity of these filtered regulons is quantified by calculating the enrichment of the regulon's target genes across a ranked list of all genes in a particular cell cluster, ordered by their expression values. This enrichment is measured as the area under the curve (AUC).

2.11 | Network-based diffusion scoring

To quantify the leverage of a specific gene on a subnetwork through its links, we used label propagation and a network diffusion algorithm, which models heat flow from seed genes along the interactions in a PPI network.[37] diffuStats, an R package that provides a collection of graph kernels and diffusion scores, and a z-scaled Monte–Carlo method were used with default parameters to calculate a diffusion score for the nodes based on pathway-specific gene sets. Information on the target molecules of drugs was retrieved from DrugBank (https://go.drugbank.com/).[38]

2.12 | Cell–cell communication analysis

T infer of cell–cell communication events using scRNA-seq data, we utilised the CellChat and LIgand–receptor ANalysis framework (LIANA) toolkits.[39,40] CellChat was used to infer the whole interaction strength between communicating cell groups, with edge weights in the resulting network proportional to these inferred interaction strengths. LIANA, a framework that integrates multiple prior knowledge resources and in silico methods, was used to generate consensus ligand–receptor (L–R) predictions of specific cell-to-cell interactions. This was achieved using the CellPhoneDB, Connectome, log2FC, NATMI and SingleCellSignalR methods and then combining their predictions. To calculate consensus score, we applied the robust rank aggregate (RRA) method to the results of these individual tools.[41] The final interaction score for each L–R pair was calculated by –log10 transforming the RRA score, which represents a probabilistic distribution. Interactions consistently ranked higher than random were assigned lower scores. The magnitude of L–R pairs was derived from the LRscore of SingleCellSignalR, with values ranging from 0 to 1.[42] Interaction specificity was determined using the specificity weight from NATMI.[43] To analyse ligand activity, we used a featured method from NicheNet.[44] This method ranks potential ligands based on how well the enrichment of a gene set of interest corresponds with a pre-existing prior model. Ligand activity was quantified by calculating the area under the precision–recall curve (AUPR) between the observed expression pattern and the relevant row from the ligand–target matrix, with the resulting corrected AUPR value representing the final ligand activity.

2.13 | Statistical analysis

For continuously distributed data, between-group comparisons were performed using unpaired t-tests. Categorical or dichotomous variables were compared using the chi-squared test or Fisher's exact test. Correlation analyses between two variables were carried out using Pearson's method.

3 | RESULTS

3.1 | Differential enrichment of IgG4-RD-associated pathways

In total, 101 upregulated DEGs were identified in salivary gland samples from IgG4-RD patients and 115 interactions within the human functional coupling interactome (Figure 1A). Twenty DEGs (19.8%), including CDH11, SNAI2 and PRRX1, were identified to be involved in the EMT process. DEG analysis conducted on bulk tissues, although informative for identifying broad quantitative shifts in gene expression, often has limited capacity to identify significant genes that are either expressed in a cell-type-specific manner, exhibit subtle transcriptional alterations, or undergo functional changes independent of mRNA abundance (e.g., via post-translational modification), and therefore could have a sparse and slack interactions between them. Thus, we prioritised disease-associated genes using the TOPAS algorithm based on DEGs as seed genes[21] and discovered additional 23 disease-associated genes, which included TGFB1 and CD47 (Figure 1A). In the functional enrichment analysis for gene sets using the GO-BP, Reactome pathway and MSigDB hallmark databases, DEGs were most enriched for extracellular matrix organisation and the EMT (Figure 1B). Key

27680622, 2026, 3, Downloaded from https://onlinelibrary.wiley.com/doi/10.1002/ctd2.70160 by Ewha Womans University Library, Wiley Online Library on [30/09/2026]. See the Terms and Conditions (https://onlinelibrary.wiley.com/terms-and-conditions) on Wiley Online Library for rules of use; OA articles are governed by the applicable Creative Commons License

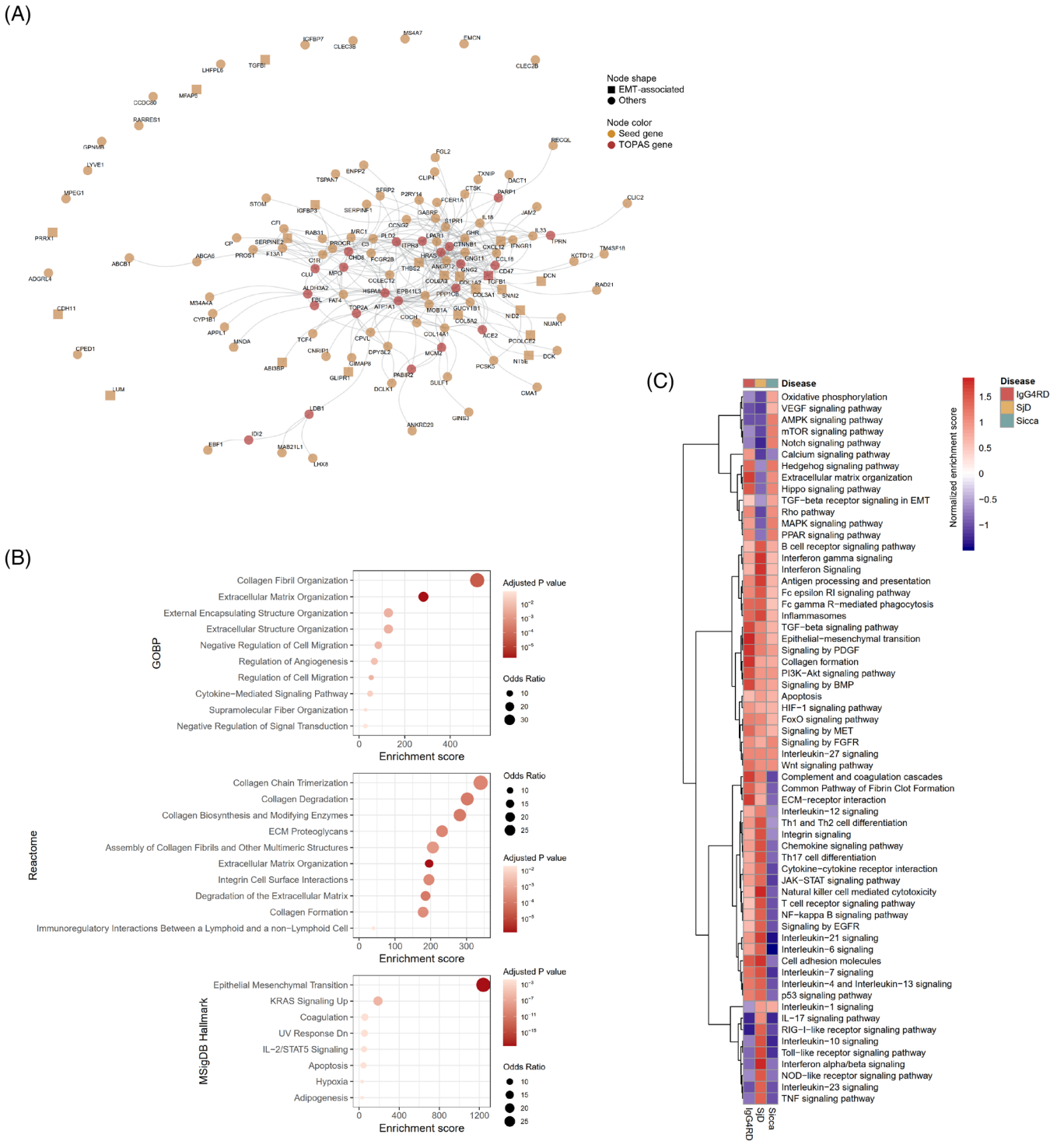


FIGURE 1 Differentially expressed genes (DEGs) and functional enrichment analysis in IgG4-related disease (IgG4-RD) salivary glands. (A) Protein–protein interaction network constructed from upregulated DEGs identified by the significance analysis of microarray (SAM) algorithm (false discovery rate [FDR] < 0.05, |fold change| > 1.5), integrated with additional disease-associated genes prioritised by the TOP–down Attachment of Seeds (TOPAS) algorithm within the FunCoup human interactome. Node shape denotes epithelial–mesenchymal transition (EMT) association; node colour indicates gene origin (seed gene vs. TOPAS-prioritised gene). (B) Functional enrichment analysis of upregulated DEGs performed using Enrichr across Gene Ontology (GO)-biological processes (BP), Reactome and Molecular Signatures Database (MSigDB) Hallmark databases. Dot size represents odds ratio; colour indicates adjusted *p*-value. (C) Heatmap of differential enrichment of IgG4-RD pathogenic pathways across IgG4-RD, Sjögren's disease (SjD), sicca syndrome and healthy controls, assessed by gene-set enrichment analysis (GSEA). Colour represents the normalised enrichment score (NES), reflecting the relative degree of pathway overrepresentation in each disease group.

27680622, 2026, 3, Downloaded from https://onlinelibrary.wiley.com/doi/10.1002/ctd2.70160 by Ewha Womans University Library, Wiley Online Library on [30/09/2026]. See the Terms and Conditions (https://onlinelibrary.wiley.com/terms-and-conditions) on Wiley Online Library for rules of use; OA articles are governed by the applicable Creative Commons License

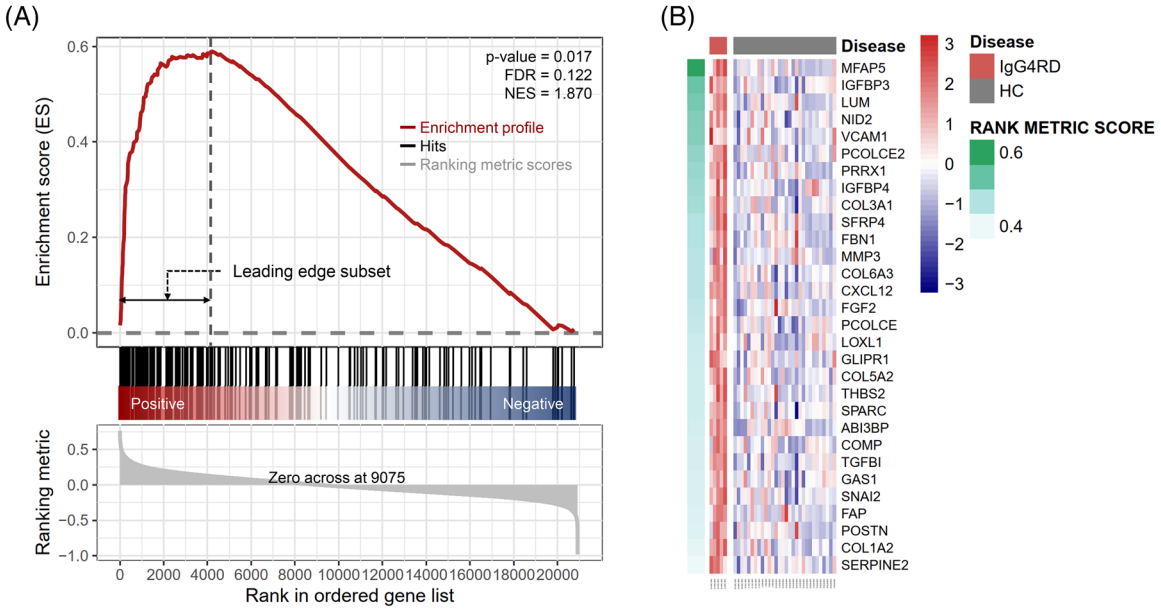


FIGURE 2 Gene-set enrichment analysis (GSEA) for epithelial–mesenchymal transition (EMT) in IgG4-related disease (IgG4-RD). (A) Preranked GSEA plot using the Molecular Signatures Database (MSigDB) Hallmark EMT gene set, run with the classic enrichment statistic and 1000 permutations, comparing IgG4-RD against healthy controls. The vertical dashed line marks the peak enrichment score defining the leading-edge subset. The barcode plot indicates hit positions of EMT genes in the ranked list, and the lower panel displays the ranking metric score. (B) Heatmap of the top 30 leading-edge genes contributing most to EMT enrichment in IgG4-RD, with expression levels compared between IgG4-RD and healthy controls. Colour indicates expression level; the right bar represents the rank metric score per gene.

DEGs and enriched BP were recapitulated using the empirical Bayes-based DEG filtering approach implemented in the limma package (Figure S2).

We collected salivary gland gene expression datasets from patients with SjD or sicca syndrome for comparison. Additionally, we conducted a literature review to compile the BP and signalling pathways involved in the pathogenesis of IgG4-RD.[4,45] Subsequently, we performed a GSEA to investigate the differential enrichment of BP and pathogenic pathways across these diseases (Figure 1C). EMT was the most enriched process (NES = 1.87, FDR = 0.122, p-value = .017) (Figure 2A). MFAP5, IGFBP3, PRRX1, CXCL12, SPARC, SNAI2 and POSTN were prioritised among 112 leading-edge genes enriched in the EMT (Figure 2B). MFAP5, IGFBP3, PRRX1, CXCL12 and SNAI2 were also elements of the DEGs (Figure 1A). PDGF-, TGFβ-, PI3K-Akt-, BMP- and Hippo signalling pathways were also enriched in IgG4-RD. Immune-inflammatory signalling pathways, including IFN and TLR signalling pathways, were enriched in SjD.

3.2 | Epithelial–mesenchymal transition towards the mesenchymal phenotype

EMT is a well-established process activated during cancer pathogenesis and tissue fibrosis.[46] Cells undergoing EMT in adult pathological tissues commonly exhibit a transitional, reversible state characterised by co-expression of both epithelial and mesenchymal markers, often referred to as 'partial EMT'.[46–48] To further understand the transitional state and regulatory balance of the EMT, we computed the EMT score using generic EMT, epithelial and mesenchymal signatures.[30,49] EMT score of IgG4-RD was significantly higher than that of SjD, sicca syndrome and healthy controls (Figure 3A). Particularly, mesenchymal score showed distinct differences across the diseases ($p = 2.42 \times 10^{-6}$), whereas epithelial scores were comparable ($p = .0817$) (Figure 3A). EMT regulation concurs with the activation of one or several EMT-transcription factors (TFs) such as SNAIL, TWIST, ZEB and PRRX families.[46,48] Expression of PRRX1, SNAI2, TWIST1, ZEB1 and ZEB2 in IgG4-RD was significantly increased compared with expression of these genes in SjD, sicca syndrome and healthy controls (Figure 3B).

EMT triggered in response to injury is associated with the activation of myofibroblasts, and extracellular matrix deposition (mainly collagen).[46,47] In cell subtype deconvolution analysis, enrichment of fibroblasts, particularly myofibroblasts, was significantly higher in IgG4-RD than in SjD, sicca syndrome and healthy controls ($p = 1.697 \times 10^{-3}$ and 7.101×10^{-4}, respectively) (Figure 3C). Pairwise comparison using unpaired t-tests revealed that myofibroblast enrichment was significantly

27680622, 2026, 3, Downloaded from https://onlinelibrary.wiley.com/doi/10.1002/ctd2.70160 by Ewha Womans University Library, Wiley Online Library on [30/09/2026]. See the Terms and Conditions (https://onlinelibrary.wiley.com/terms-and-conditions) on Wiley Online Library for rules of use; OA articles are governed by the applicable Creative Commons License

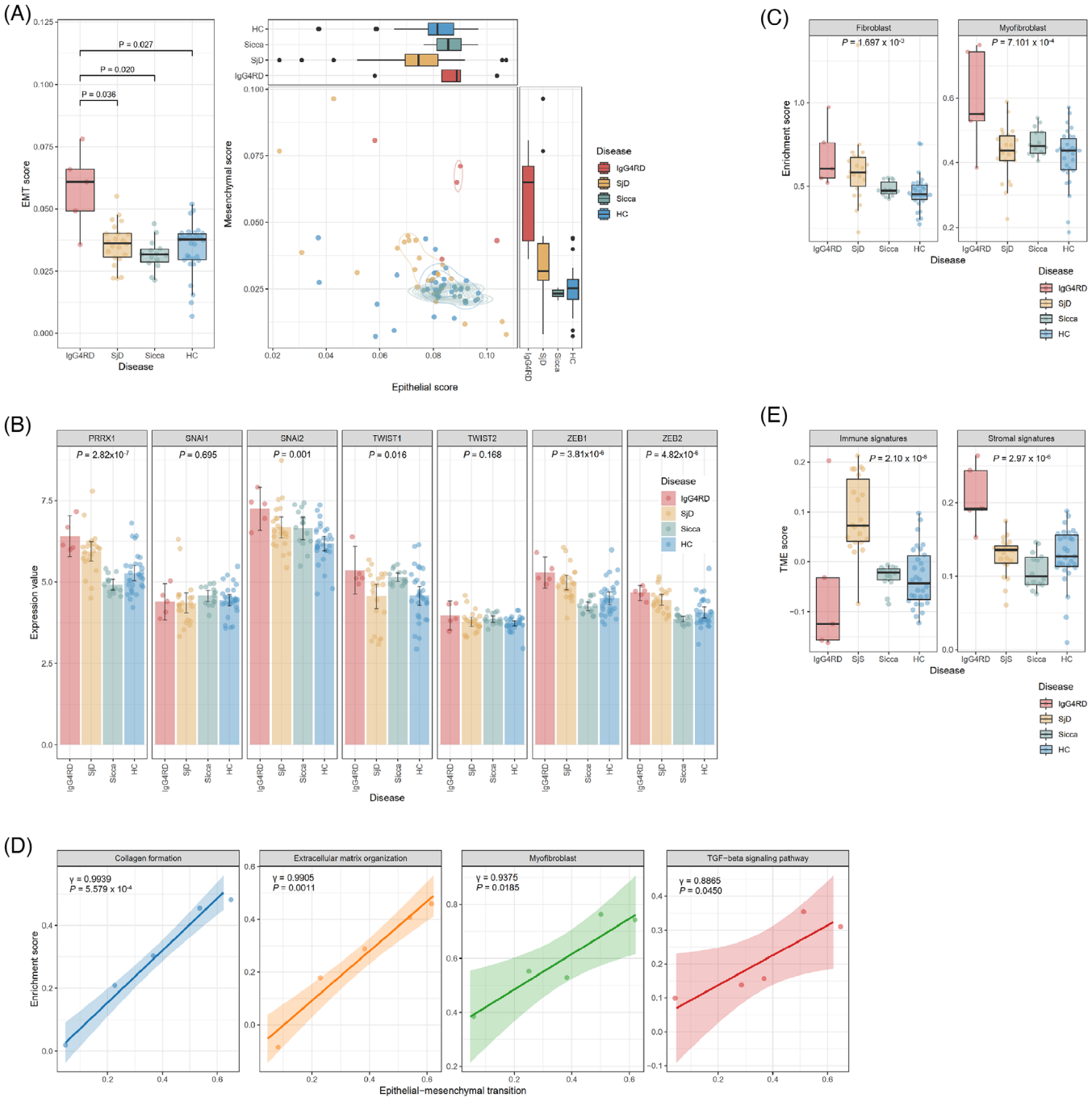


FIGURE 3 Epithelial–mesenchymal transition (EMT) scores and EMT-associated molecular signatures across diseases. (A) Generic EMT, epithelial and mesenchymal scores computed using the AUCell algorithm with Molecular Signatures Database (MSigDB) Hallmark and previously published EMT signature gene sets, compared across disease groups. Left boxplot shows generic EMT scores; right scatter plot shows epithelial versus mesenchymal scores per sample. (B) Expression levels of EMT-transcription factors across disease groups, compared by analysis of variance (ANOVA) test. (C) Fibroblast and myofibroblast enrichment scores estimated by the digital sorting algorithm (DSA) cell-type deconvolution method and compared across groups. Scores across the groups were compared by ANOVA test. (D) Pearson correlation analysis between per-sample EMT enrichment scores and scores of collagen formation, extracellular matrix organisation, myofibroblasts and transforming growth factor-β (TGF-β) signalling pathway. (E) Stromal and immune signature scores estimated by the ESTIMATE algorithm and compared across disease groups. Scores across the groups are compared by ANOVA test.

27680622, 2026, 3, Downloaded from https://onlinelibrary.wiley.com/doi/10.1002/ctd2.70160 by Ewha Womans University Library, Wiley Online Library on [30/09/2026]. See the Terms and Conditions (https://onlinelibrary.wiley.com/terms-and-conditions) on Wiley Online Library for rules of use; OA articles are governed by the applicable Creative Commons License

greater in IgG4-RD than in SjD ($p = .0028$), whereas fibroblast abundance was comparable between the two groups ($p = .409$) (Figure S3). In correlative analysis, EMT was significantly correlated with collagen formation and extracellular matrix organisation ($\gamma = 0.9939$, $p = 5.579 \times 10^{-4}$ and $\gamma = 0.9905$, $p = .0011$) (Figure 3D). EMT also has a significant correlation with myofibroblasts ($\gamma = 0.9375$, $p = .0185$) and the TGF-β signalling pathway ($\gamma = 0.8865$, $p = .0450$).

IgG4-RD exhibits tumour-like features in its pathology as well as clinical manifestations.[2,4] Expanded stromal cells and infiltrating immune cells form the tumour microenvironment, which impacts tumour aggressiveness and treatment response.[50,51] EMT and extracellular matrix remodelling are also active processes within this environment.[50,51] We estimated the fraction of stromal and immune cells based on this line of reasoning using the ESTIMATE algorithm.[32] The stromal signature score was significantly higher in IgG4-RD than in SjD, sicca syndrome and healthy controls ($p = 2.10 \times 10^{-8}$), whereas immune signature score was highest in SjD ($p = 2.97 \times 10^{-6}$) (Figure 3E).

3.3 | Cell–cell interactions among immune cells in IgG4-RD

We imported GSE2428778, a scRNA-seq dataset of salivary gland tissue obtained from patients with IgG4-RD.[15] In cell-type-specific, pathway-driven enrichment analysis using GVSA, fibroblasts showed the strongest enriched signals for the EMT, extracellular matrix organisation and signalling by PDGF as compared to other cell types (Figure 4A). In GRN analysis using SCENIC, TCF7L2, NFIC, TWIST1, PLAGL1 and ZEB1 were identified as key regulons in fibroblasts (Figure 4A). Next, we investigated cell-type-specific features and the interaction network among cell types using CellChat,[39] LIANA[40] and NicheNet[44] toolkits. Fibroblasts were the major cell type sending and receiving the signals in cell–cell interacting network (Figure 4B). We focused on the relationship between fibroblasts and CD19$^+$ B cells because a recent clinical trial of B-cell-depletion therapy using inebilizumab targeting CD19 in patients with active IgG4-RD reported promising results.[5] In UMAP, clusters annotated with naïve B cells expressed CD19 and were the major cell type expressing TGF-β1 and CXCR4 together with cytotoxic or regulatory T cells (Figure 4C). In L–R pairing analysis, CD19$^+$ B cells stimulated fibroblasts through TGFB1–TGFBR3 interaction, which was further assisted by co-receptors including LPP, EGFR, ENG, CAV1 and SDC2 (Figure 5A). We examined aggregated ranks of L–R interactions between two cell types using a robust rank aggregation method in the LIANA toolkit and assessed the predictability of the prioritised ligands for the EMT gene set compared to the background of expressed genes in fibroblasts using ligand activity analysis in the NicheNet toolkit. TGFB1 ligation showed the strongest activity for EMT signatures in fibroblasts (Figure 5B). In turn, fibroblasts support CD19$^+$ B cells primarily through CXCL14–CXCR4 and CXCL12–CXCR4 interactions (Figure 5C). We assessed the activity of the prioritised ligands for chemokine signalling pathway genes in CD19$^+$ B cells. CXCL12 ligation from fibroblasts to CD19$^+$ B cells showed the highest ligand activity (Figure 5D). Cytotoxic T cells and regulatory T cells were the primary subsets interacting with fibroblasts (Figure 4B). Notably, regulatory T cells were found to stimulate fibroblasts through multiple ligands, including TGFB1, calmodulin family members (CALMs) and CD40LG. TGFB1 ligation had the strongest activity for EMT signatures in fibroblasts (Figure S4).

4 | DISCUSSION

In this study, we retrieved the gene expression profiles of patients with IgG4-RD affecting salivary glands at bulk and single-cell levels and analysed these profiles to elucidate the cellular and molecular features of IgG4-RD, with a particular focus on fibrotic processes. We identified EMT as a key pathologic process in the fibro-inflammatory microenvironment of IgG4-RD and found that the EMT closely correlated with extracellular matrix organisation and TGF-β signalling pathways. Fibroblasts were the main cell subset enriched in the EMT signature, while CD19$^+$ B cells, along with cytotoxic T cells, and regulatory T cells, were the main sources of TGF-β1. The EMT in fibroblasts was activated mainly by TGF-β1 from CD19$^+$ B cells and in turn, fibroblasts supported CD19$^+$ B cells via CXCL14–CXCR4 and CXCL12–CXCR4 interactions.

EMT was the most enriched pathological process in salivary gland IgG4-RD. Organs commonly affected by IgG4-RD including salivary glands, lacrimal glands and the pancreas are primarily composed of epithelial cells and could therefore be more susceptible to the EMT. EMT is a partial but direct contributor to the fibroblast and myofibroblast pools during fibrogenesis.[52] Lineage-tagging experiments and bone marrow transplant studies have demonstrated that, during the progression of kidney fibrosis in mice, approximately 12% of fibroblasts originate from the bone marrow, while about 30% arise through the EMT of tubular epithelial cells of the kidney.[52] Fibroblasts are likely derived partly from epithelial cells in salivary gland IgG4-RD because fibroblasts subsets were the most enriched for the EMT process. These fibroblasts may have pro-fibrosing capacity because they exhibited increased

27680622, 2026, 3, Downloaded from https://onlinelibrary.wiley.com/doi/10.1002/ctd2.70160 by Ewha Womans University Library, Wiley Online Library on [30/09/2026]. See the Terms and Conditions (https://onlinelibrary.wiley.com/terms-and-conditions) on Wiley Online Library for rules of use; OA articles are governed by the applicable Creative Commons License

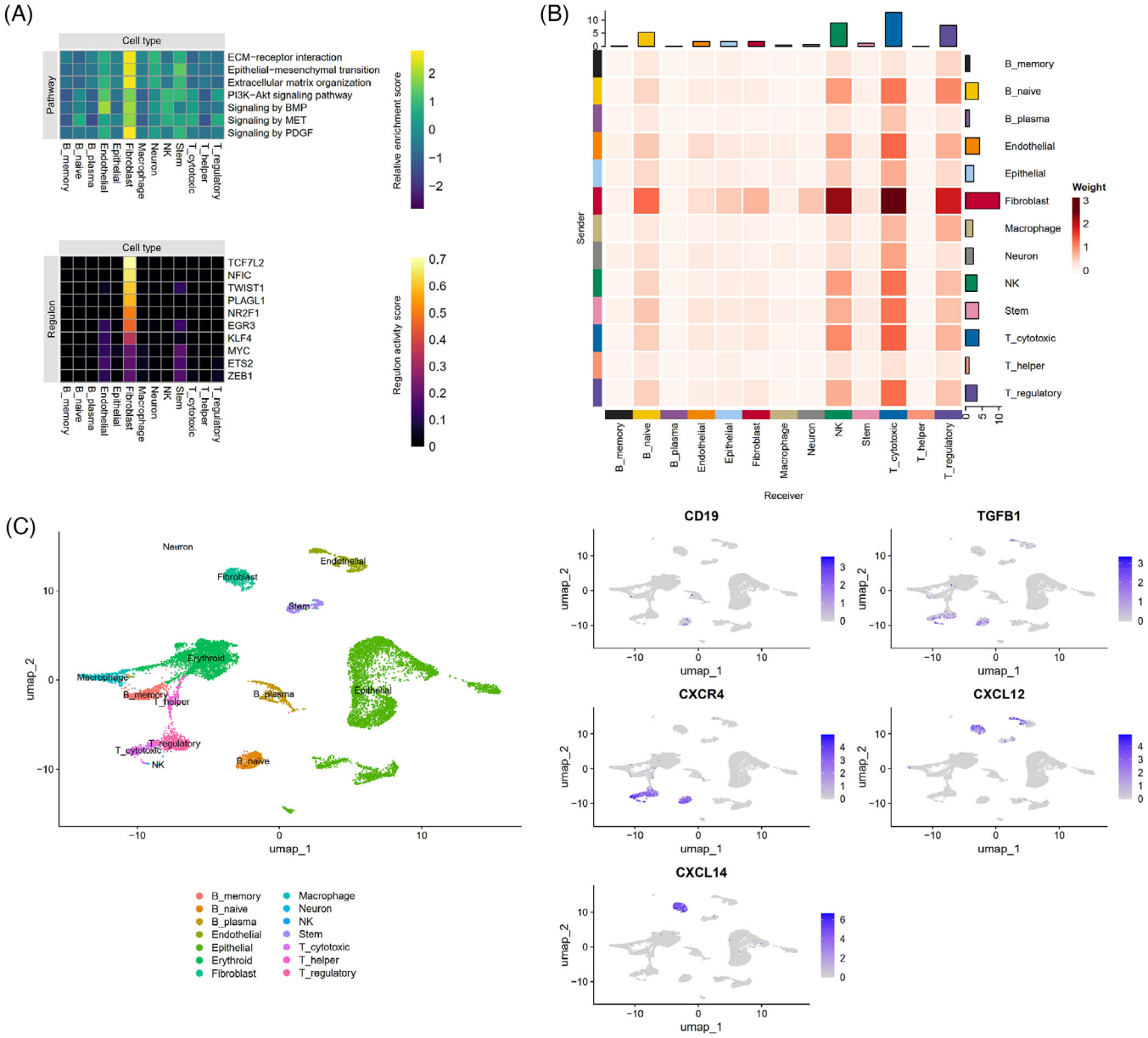


FIGURE 4 Single-cell level molecular signatures and cell–cell communication network in IgG4-related disease (IgG4-RD). (A) Upper: cell-type-specific enrichment of fibrosis-associated pathways assessed by gene-set variation analysis (GSVA) using single-cell RNA sequencing (scRNA-seq) data from IgG4-RD salivary glands (GSE242778). All *p*-value for the pathway enrichment scores across the cell types were $<2 \times 10^{-16}$ by analysis of variance (ANOVA). Lower: regulon activity scores in each cell subtype inferred by SCENIC, identifying key transcriptional regulators active in fibroblasts. Regulon activity scores represent the proportion of cells within each cell type in which the regulon is active, as determined by the SCENIC binary activity matrix; ranging from 0 to 1, with higher values indicating greater regulon activity in a certain cell type. (B) Cell–cell communication network inferred by CellChat, with edge width proportional to interaction strength, illustrating the overall signalling topology among annotated cell types. (C) Left: UMAP of scRNA-seq data with cell-type annotations determined by SingleR and CellTypist. Right: feature plots show the expression distribution of CD19, TGFB1, CXCR4, CXCL12 and CXCL14 across cell types, with purple intensity representing relative expression level.

expression of EMT-TFs, including PRRX1, SNAI2, TWIST1, ZEB1 and ZEB2, favouring the myofibroblast phenotype. In gene regulatory analysis at the single-cell level, TCF7L2, NFIC and PLAGL1, in addition to TWIST1 and ZEB1, were identified as key regulons in fibroblasts. TCF7L2, NFIC and PLAGL1 have been implicated in the EMT process, contributing to cancer metastasis.[53–55] There is strong evidence supporting the role of sustained and irreversible EMT as a driver of fibrosis independent of induction from epithelial cells to fibroblasts. EMT promotes the secretion of TGF-β and inflammatory cytokines from damaged epithelial cells to respectively promote myofibroblast

27680622, 2026, 3, Downloaded from https://onlinelibrary.wiley.com/doi/10.1002/ctd2.70160 by Ewha Womans University Library, Wiley Online Library on [30/09/2026]. See the Terms and Conditions (https://onlinelibrary.wiley.com/terms-and-conditions) on Wiley Online Library for rules of use; OA articles are governed by the applicable Creative Commons License

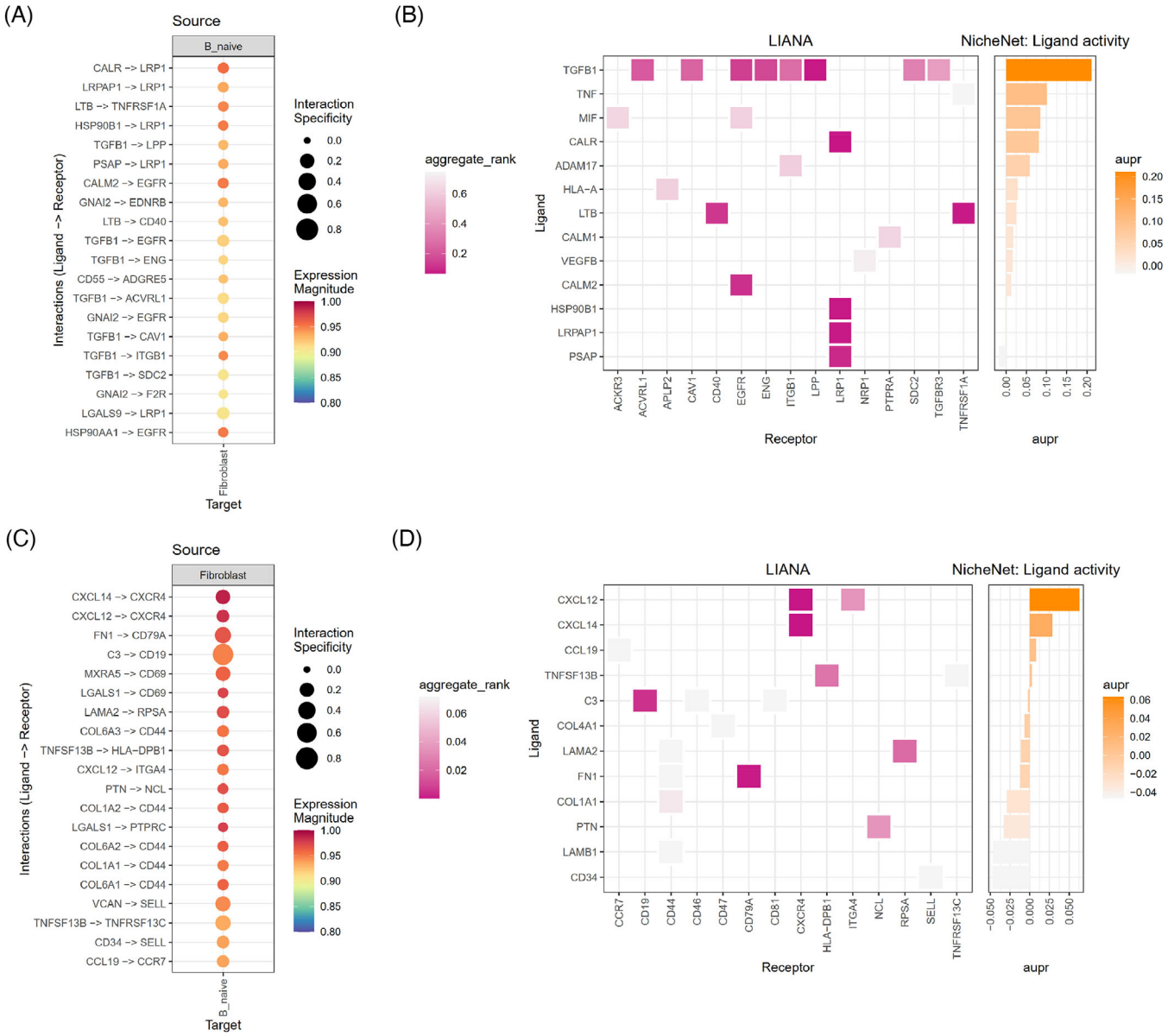


FIGURE 5 Ligand–receptor interaction analysis between CD19$^+$ B cells and fibroblasts. (A) Ligand–receptor pairs from CD19$^+$ B cells (source) to fibroblasts (target) identified by LIgand–receptor ANalysis framework (LIANA), which integrates five methods (CellPhoneDB, Connectome, log2FC, NATMI and SingleCellSignalR) and ranks pairs by robust rank aggregation. Dot size indicates interaction specificity; colour represents expression magnitude. (B) Left: aggregate rank heatmap of ligand–receptor pairs between CD19$^+$ B cells and fibroblasts by LIANA. Right: ligand activity assessed by NicheNet using area under the precision–recall curve (AUPR) against the epithelial–mesenchymal transition (EMT) gene set expressed in fibroblasts. (C) Ligand–receptor pairs from fibroblasts (source) to CD19$^+$ B cells (target), ranked by the same LIANA framework. (D) Left: aggregate rank heatmap of ligand–receptor pairs between fibroblasts and CD19$^+$ B cells. Right: NicheNet ligand activity assessed by AUPR against the chemokine signalling gene set expressed in CD19$^+$ B cells.

activation and immune inflammation, leading to tissue fibrosis.[46] We found that the EMT showed a strong correlative relationship with myofibroblasts, extracellular matrix organisation and TGF-β signalling despite the small size of our IgG4-RD sample.

Glucocorticoids are the recommended first-line therapy for IgG4-RD if there are no contraindications; response rates to glucocorticoids have been estimated to exceed 85%.[4] They are also effective in reducing relapse rates when used as maintenance therapy.[56,57] Glucocorticoids were reported to ameliorate the TGF-β1-mediated EMT of the airway epithelium through MAPK and Snail/Slug signalling pathways.[58,59] The therapeutic efficacy of glucocorticoids in IgG4-RD might be attributable partly to suppression of the EMT.

27680622, 2026, 3, Downloaded from https://onlinelibrary.wiley.com/doi/10.1002/ctd2.70160 by Ewha Womans University Library, Wiley Online Library on [30/09/2026]. See the Terms and Conditions (https://onlinelibrary.wiley.com/terms-and-conditions) on Wiley Online Library for rules of use; OA articles are governed by the applicable Creative Commons License

Based on current knowledge, oligoclonally expanded B cells and plasmablasts contribute to fibroblast activation through secretion of PDGF-β and LOXL2.[4,6,45] TGF-β, the key cytokine mediating the EMT and fibroblast activation, is known to be derived from infiltrated CD4$^+$ T cells and macrophages in the affected tissues of IgG4-RD.[4,45,60] B-cell depletion using rituximab attenuated serological biomarkers of fibrosis and myofibroblast activation in patients with IgG4-RD[61] and the good outcomes achieved by depleting B cells with inebilizumab in IgG4-RD patients further underscore the importance of B cells in the pathophysiology of IgG4-RD.[5,9] In our single-cell analysis, we identified CD19$^+$ B cells, together with cytotoxic and regulatory T cells, as major sources of TGF-β1. B cells are not usually the source of pathologic TGF-β in fibrotic diseases though B cells produce relatively low levels of both the precursor and active forms of TGF-β under physiological, healthy conditions.[62,63] Possible roles of TGF-β-producing B cells in some autoimmune diseases, cancer and allergic diseases have been investigated,[63] but TGF-β-producing CD19$^+$ B cells in IgG4-RD is a novel finding. It is unclear how similar or different the TGF-β^+ CD19$^+$ B cells in IgG4-RD are from the previously designated TGF-β-secreting regulatory B cells.[63] It would be intriguing to investigate a potential pathogenic link between IgG4 production and TGF-β generation from B-lineage cells in IgG4-RD.

Typical microscopic findings of IgG4-RD include dense and usually tumefactive lymphoplasmacytic infiltrates associated with a variable degree of fibrosclerosis and increased numbers of IgG4-expressing tissue cells. Storiform fibrosis is a characteristic finding of IgG4-RD and involves spindle cells, which are either fibroblasts or myofibroblasts.[64,65] Storiform fibrosis is typically buried within the lymphoplasmacytic infiltrates, which comprise B and T lymphocytes.[64,65] This implies that fibroblasts are contiguous to B cells and have high chance of close interactions in the IgG4-RD microenvironment. In cell–cell communication analysis, TGF-β ligation was the most active signal that CD19$^+$ B cells delivered to fibroblasts. This suggests that anti-CD19 therapy may have therapeutic efficacy in IgG4-RD considering the major role of TGF-β in the EMT process and tissue fibrosis. Conversely, we found that fibroblasts deliver CXCR4 signals to CD19$^+$ B cells by ligation of CXCL12 and CXCL14. The CXCR4 axis is critically involved in B-cell responses, including antibody production, and also promotes B-cell viability.[66] Therefore, through this feed-forward interaction, B cells and fibroblasts might form the backbone of the IgG4 deposition and fibrotic process in IgG4-RD.

This study has several limitations that need to be addressed. First, we did not investigate the relationship between molecular features and clinical or histopathological characteristics of IgG4-RD due to insufficiently detailed clinical and histopathological information at the individual level. Second, transcriptomic data were available for only five salivary gland tissue samples from the data repository. A small sample size is susceptible to selection bias. To mitigate this effect, a sufficient number of healthy control samples were secured for comparison. IgG4-RD is a rare and unique fibroinflammatory disease, and tissue samples are extremely scarce. However, despite these limitations, these samples are the only consistent source of tissue for new investigative analyses. A third limitation of our study is that our findings are based on a cohort of patients with IgG4-RD primarily affecting the salivary glands. Therefore, future studies are required to determine if similar results can be replicated in IgG4-RD affecting other tissues or organs.

Our major findings are the EMT is an active process involved in the fibrosis of IgG4-RD and that TGF-β1, a key cytokine that drives the EMT, is produced by CD19$^+$ B cells. Furthermore, we revealed that a supportive interaction between CD19$^+$ B cells and fibroblasts that appears to play a pivotal role in the pathogenesis of IgG4-RD. The role of deposited IgG4 in IgG4-RDs remains enigmatic.[67] Within the tumour microenvironment, EMT confers cancer cells with increased tumour-initiating and metastatic potential, as well as greater resistance to various therapeutic regimens. Similarly, the TGF-β1-mediated EMT in IgG4-RD may have diverse impacts on disease pathobiology and the clinical response to therapy. Our findings not only address a significant knowledge gap, but also provide supporting evidence for the therapeutic value of B-cell-depletion therapy in IgG4-RD and offer novel insights for developing effective strategies.

AUTHOR CONTRIBUTIONS

Conceptualisation: Ki-Jo Kim. *Methodology*: Ki-Jo Kim. *Data analysis*: In-Woon Baek and Ki-Jo Kim. *Supervision*: Ki-Jo Kim. *Writing—original draft*: In-Woon Baek and Ki-Jo Kim. *Writing—review and editing*: In-Woon Baek, Kyung-Su Park and Ki-Jo Kim. *Guarantor*: Ki-Jo Kim.

FUNDING INFORMATION

No specific funding was received from any funding bodies in the public, commercial or not-for-profit sectors to carry out the work described in this manuscript.

CONFLICT OF INTEREST STATEMENT

The authors declare they have no conflicts of interest.

DATA AVAILABILITY STATEMENT

All raw data are available in a public, open-access repository. The data have been deposited in the Gene Expression Omnibus repository under accession numbers GSE3526, GSE7307, GSE40568, GSE40611 and GSE242778. Metadata

27680622, 2026, 3, Downloaded from https://onlinelibrary.wiley.com/doi/10.1002/ctd2.70160 by Ewha Womans University Library, Wiley Online Library on [30/09/2026]. See the Terms and Conditions (https://onlinelibrary.wiley.com/terms-and-conditions) on Wiley Online Library for rules of use; OA articles are governed by the applicable Creative Commons License

and interim processed data are available upon reasonable request from the corresponding author.

ETHICS STATEMENT

This study complies with the Helsinki Declaration and all raw data used in this study are available in a public, open-access repository and only summary-level datasets without participants were used.

ORCID

In-Woon Baek https://orcid.org/0000-0002-2261-4287
Kyung-Su Park https://orcid.org/0000-0003-0020-003X
Ki-Jo Kim https://orcid.org/0000-0002-3598-2396

REFERENCES

1. Wallace ZS, Naden RP, Chari S, et al. The 2019 American College of Rheumatology/European League Against Rheumatism classification criteria for IgG4-related disease. *Ann Rheum Dis*. 2020;79(1):77-87.
2. Stone JH, Zen Y, Deshpande V. IgG4-related disease. *N Engl J Med*. 2012;366(6):539-551.
3. Chen LYC, Mattman A, Seidman MA, Carruthers MN. IgG4-related disease: what a hematologist needs to know. *Haematologica*. 2019;104(3):444-455.
4. Peyronel F, Della-Torre E, Maritati F, et al. IgG4-related disease and other fibro-inflammatory conditions. *Nat Rev Rheumatol*. 2025;21(5):275-290.
5. Stone JH, Khosroshahi A, Zhang W, et al. Inebilizumab for treatment of IgG4-related disease. *N Engl J Med*. 2025;392(12):1168-1177.
6. Della-Torre E, Rigamonti E, Perugino C, et al. B lymphocytes directly contribute to tissue fibrosis in patients with IgG(4)-related disease. *J Allergy Clin Immunol*. 2020;145(3):968-981.e914.
7. Carruthers MN, Topazian MD, Khosroshahi A, et al. Rituximab for IgG4-related disease: a prospective, open-label trial. *Ann Rheum Dis*. 2015;74(6):1171-1177.
8. Ebbo M, Grados A, Samson M, et al. Long-term efficacy and safety of rituximab in IgG4-related disease: data from a French nationwide study of thirty-three patients. *PLoS One*. 2017;12(9):e0183844.
9. Spiera R. Beyond glucocorticoids for IgG4-related disease. *N Engl J Med*. 2025;392(12):1232-1233.
10. Zhao M, Wang L, Wang M, et al. Targeting fibrosis, mechanisms and clinical trials. *Signal Transduct Target Ther*. 2022;7(1):206.
11. Podolanczuk AJ, Thomson CC, Remy-Jardin M, et al. Idiopathic pulmonary fibrosis: state of the art for 2023. *Eur Respir J*. 2023;61(4):2200957.
12. Pope JE, Denton CP, Johnson SR, Fernandez-Codina A, Hudson M, Nevskaya T. State-of-the-art evidence in the treatment of systemic sclerosis. *Nat Rev Rheumatol*. 2023;19(4):212-226.
13. Tsuboi H, Nakai Y, Iizuka M, et al. DNA microarray analysis of labial salivary glands in IgG4-related disease: comparison with Sjögren's syndrome. *Arthritis Rheumatol*. 2014;66(10):2892-2899.
14. Horvath S, Nazmul-Hossain AN, Pollard RP, et al. Systems analysis of primary Sjögren's syndrome pathogenesis in salivary glands identifies shared pathways in human and a mouse model. *Arthritis Res Ther*. 2012;14(6):R238.
15. Tanaka S, Yamamoto T, Iwata A, et al. Single-cell RNA sequencing of submandibular gland reveals collagen type XV-positive fibroblasts as a disease-characterizing cell population of IgG4-related disease. *Arthritis Res Ther*. 2024;26(1):55.
16. Gautier L, Cope L, Bolstad BM, Irizarry RA. affy—analysis of Affymetrix GeneChip data at the probe level. *Bioinformatics*. 2004;20(3):307-315.
17. Johnson WE, Li C, Rabinovic A. Adjusting batch effects in microarray expression data using empirical Bayes methods. *Biostatistics*. 2007;8(1):118-127.
18. Chen C, Grennan K, Badner J, et al. Removing batch effects in analysis of expression microarray data: an evaluation of six batch adjustment methods. *PLoS One*. 2011;6(2):e17238.
19. Müller C, Schillert A, Röthemeier C, et al. Removing batch effects from longitudinal gene expression—quantile normalization plus ComBat as best approach for microarray transcriptome data. *PLoS One*. 2016;11(6):e0156594.
20. Tusher VG, Tibshirani R, Chu G. Significance analysis of microarrays applied to the ionizing radiation response. *Proc Natl Acad Sci U S A*. 2001;98(9):5116-5121.
21. Buzzao D, Castresana-Aguirre M, Guala D, Sonnhammer ELL. TOPAS, a network-based approach to detect disease modules in a top–down fashion. *NAR Genom Bioinform*. 2022;4(4):lqac093.
22. Evangelista JE, Xie Z, Marino GB, Nguyen N, Clarke DJB, Ma'ayan A. Enrichr-KG: bridging enrichment analysis across multiple libraries. *Nucleic Acids Res*. 2023;51(W1):W168-W179.
23. Subramanian A, Tamayo P, Mootha VK, et al. Gene set enrichment analysis: a knowledge-based approach for interpreting genome-wide expression profiles. *Proc Natl Acad Sci U S A*. 2005;102(43):15545-15550.
24. Kanehisa M, Furumichi M, Tanabe M, Sato Y, Morishima K. KEGG: new perspectives on genomes, pathways, diseases and drugs. *Nucleic Acids Res*. 2017;45(D1):D353-D361.
25. Ashburner M, Ball CA, Blake JA, et al. Gene ontology: tool for the unification of biology. The Gene Ontology Consortium. *Nat Genet*. 2000;25(1):25-29.
26. Milacic M, Beavers D, Conley P, et al. The Reactome Pathway Knowledgebase 2024. *Nucleic Acids Res*. 2024;52(D1):D672-D678.
27. Liberzon A, Birger C, Thorvaldsdóttir H, Ghandi M, Mesirov JP, Tamayo P. The Molecular Signatures Database (MSigDB) hallmark gene set collection. *Cell Syst*. 2015;1(6):417-425.
28. Hänzelmann S, Castelo R, Guinney J. GSVA: gene set variation analysis for microarray and RNA-seq data. *BMC Bioinformatics*. 2013;14:7.
29. Zhong Y, Wan YW, Pang K, Chow LM, Liu Z. Digital sorting of complex tissues for cell type-specific gene expression profiles. *BMC Bioinformatics*. 2013;14:89.
30. Panchy N, Watanabe K, Takahashi M, Willems A, Hong T. Comparative single-cell transcriptomes of dose and time dependent epithelial–mesenchymal spectrums. *NAR Genom Bioinform*. 2022;4(3):lqac072.
31. Aibar S, González-Blas CB, Moerman T, et al. SCENIC: single-cell regulatory network inference and clustering. *Nat Methods*. 2017;14(11):1083-1086.
32. Yoshihara K, Shahmoradgoli M, Martínez E, et al. Inferring tumour purity and stromal and immune cell admixture from expression data. *Nat Commun*. 2013;4:2612.

27680622, 2026, 3, Downloaded from https://onlinelibrary.wiley.com/doi/10.1002/ctd2.70160 by Ewha Womans University Library, Wiley Online Library on [30/09/2026]. See the Terms and Conditions (https://onlinelibrary.wiley.com/terms-and-conditions) on Wiley Online Library for rules of use; OA articles are governed by the applicable Creative Commons License

33. Buzzao D, Persson E, Guala D, Sonnhammer ELL. FunCoup 6: advancing functional association networks across species with directed links and improved user experience. *Nucleic Acids Res*. 2025;53(D1):D658-D671.
34. Hao Y, Hao S, Andersen-Nissen E, et al. Integrated analysis of multimodal single-cell data. *Cell*. 2021;184(13):3573-3587.e3529.
35. Aran D, Looney AP, Liu L, et al. Reference-based analysis of lung single-cell sequencing reveals a transitional profibrotic macrophage. *Nat Immunol*. 2019;20(2):163-172.
36. Conde CD, Xu C, Jarvis LB, et al. Cross-tissue immune cell analysis reveals tissue-specific features in humans. *Science*. 2022;376(6594):eabl5197.
37. Picart-Armada S, Thompson WK, Buil A, Perera-Lluna A. diffuStats: an R package to compute diffusion-based scores on biological networks. *Bioinformatics*. 2018;34(3):533-534.
38. Knox C, Wilson M, Klinger CM, et al. DrugBank 6.0: the DrugBank Knowledgebase for 2024. *Nucleic Acids Res*. 2024;52(D1):D1265-D1275.
39. Jin S, Guerrero-Juarez CF, Zhang L, et al. Inference and analysis of cell–cell communication using CellChat. *Nat Commun*. 2021;12(1):1088.
40. Dimitrov D, Türei D, Garrido-Rodriguez M, et al. Comparison of methods and resources for cell–cell communication inference from single-cell RNA-seq data. *Nat Commun*. 2022;13(1):3224.
41. Kolde R, Laur S, Adler P, Vilo J. Robust rank aggregation for gene list integration and meta-analysis. *Bioinformatics*. 2012;28(4):573-580.
42. Cabello-Aguilar S, Alame M, Kon-Sun-Tack F, Fau C, Lacroix M, Colinge J. SingleCellSignalR: inference of intercellular networks from single-cell transcriptomics. *Nucleic Acids Res*. 2020;48(10):e55.
43. Hou R, Denisenko E, Ong HT, Ramilowski JA, Forrest ARR. Predicting cell-to-cell communication networks using NATMI. *Nat Commun*. 2020;11(1):5011.
44. Browaeys R, Saelens W, Saeys Y. NicheNet: modeling intercellular communication by linking ligands to target genes. *Nat Methods*. 2020;17(2):159-162.
45. Löhr JM, Vujasinovic M, Rosendahl J, Stone JH, Beuers U. IgG4-related diseases of the digestive tract. *Nat Rev Gastroenterol Hepatol*. 2022;19(3):185-197.
46. Youssef KK, Nieto MA. Epithelial–mesenchymal transition in tissue repair and degeneration. *Nat Rev Mol Cell Biol*. 2024;25(9):720-739.
47. Nieto MA, Huang RY, Jackson RA, Thiery JP. EMT: 2016. *Cell*. 2016;166(1):21-45.
48. Yang J, Antin P, Berx G, et al. Guidelines and definitions for research on epithelial–mesenchymal transition. *Nat Rev Mol Cell Biol*. 2020;21(6):341-352.
49. Tan TZ, Miow QH, Miki Y, et al. Epithelial–mesenchymal transition spectrum quantification and its efficacy in deciphering survival and drug responses of cancer patients. *EMBO Mol Med*. 2014;6(10):1279-1293.
50. de Visser KE, Joyce JA. The evolving tumor microenvironment: from cancer initiation to metastatic outgrowth. *Cancer Cell*. 2023;41(3):374-403.
51. Yuan S, Almagro J, Fuchs E. Beyond genetics: driving cancer with the tumour microenvironment behind the wheel. *Nat Rev Cancer*. 2024;24(4):274-286.
52. Kalluri R, Weinberg RA. The basics of epithelial–mesenchymal transition. *J Clin Invest*. 2009;119(6):1420-1428.
53. Karve K, Netherton S, Deng L, Bonni A, Bonni S. Regulation of epithelial–mesenchymal transition and organoid morphogenesis by a novel TGFβ-TCF7L2 isoform-specific signaling pathway. *Cell Death Dis*. 2020;11(8):704.
54. Wang H, Shi X, Wu S. miR-550a-3/NFIC plays a driving role in esophageal squamous cell cancer cells proliferation and metastasis partly through EMT process. *Mol Cell Biochem*. 2020;472(1–2):115-123.
55. Wu L, Zhou Z, Han S, et al. PLAGL2 promotes epithelial–mesenchymal transition and mediates colorectal cancer metastasis via β-catenin-dependent regulation of ZEB1. *Br J Cancer*. 2020;122(4):578-589.
56. Masaki Y, Matsui S, Saeki T, et al. A multicenter phase II prospective clinical trial of glucocorticoid for patients with untreated IgG4-related disease. *Mod Rheumatol*. 2017;27(5):849-854.
57. Masamune A, Nishimori I, Kikuta K, et al. Randomised controlled trial of long-term maintenance corticosteroid therapy in patients with autoimmune pancreatitis. *Gut*. 2017;66(3):487-494.
58. Zhang L, Lei W, Wang X, Tang Y, Song J. Glucocorticoid induces mesenchymal-to-epithelial transition and inhibits TGF-β1-induced epithelial-to-mesenchymal transition and cell migration. *FEBS Lett*. 2010;584(22):4646-4654.
59. Yang HW, Lee SA, Shin JM, Park IH, Lee HM. Glucocorticoids ameliorate TGF-β1-mediated epithelial-to-mesenchymal transition of airway epithelium through MAPK and Snail/Slug signaling pathways. *Sci Rep*. 2017;7(1):3486.
60. Rovati L, Kaneko N, Pedica F, et al. Mer tyrosine kinase as a possible link between resolution of inflammation and tissue fibrosis in IgG4-related disease. *Rheumatology (Oxford)*. 2021;60(10):4929-4941.
61. Della-Torre E, Feeney E, Deshpande V, et al. B-cell depletion attenuates serological biomarkers of fibrosis and myofibroblast activation in IgG4-related disease. *Ann Rheum Dis*. 2015;74(12):2236-2243.
62. Frangogiannis N. Transforming growth factor-β in tissue fibrosis. *J Exp Med*. 2020;217(3):e20190103.
63. Huai G, Markmann JF, Deng S, Rickert CG. TGF-β-secreting regulatory B cells: unsung players in immune regulation. *Clin Transl Immunology*. 2021;10(4):e1270.
64. Czarnywojtek A, Agaimy A, Pietrończyk K, et al. IgG4-related disease: an update on pathology and diagnostic criteria with a focus on salivary gland manifestations. *Virchows Arch*. 2024;484(3):381-399.
65. Deshpande V, Zen Y, Chan JK, et al. Consensus statement on the pathology of IgG4-related disease. *Mod Pathol*. 2012;25(9):1181-1192.
66. Giorgiutti S, Rottura J, Korganow AS, Gies V. CXCR4: from B-cell development to B cell-mediated diseases. *Life Sci Alliance*. 2024;7(6):e202302465. Doi:10.26508/lsa.202302465
67. Rispens T, Huijbers MG. The unique properties of IgG4 and its roles in health and disease. *Nat Rev Immunol*. 2023;23(11):763-778.

27680622, 2026, 3, Downloaded from https://onlinelibrary.wiley.com/doi/10.1002/ctd2.70160 by Ewha Womans University Library, Wiley Online Library on [30/09/2026]. See the Terms and Conditions (https://onlinelibrary.wiley.com/terms-and-conditions) on Wiley Online Library for rules of use; OA articles are governed by the applicable Creative Commons License

SUPPORTING INFORMATION

Additional supporting information can be found online in the Supporting Information section at the end of this article.

How to cite this article: Baek I-W, Park K-S, Kim K-J. TGF-β1-driven epithelial–mesenchymal transition mediates the fibrotic process in IgG4-related disease. *Clin Transl Disc*. 2026;6:e70160. https://doi.org/10.1002/ctd2.70160

27680622, 2026, 3, Downloaded from https://onlinelibrary.wiley.com/doi/10.1002/ctd2.70160 by Ewha Womans University Library, Wiley Online Library on [30/09/2026]. See the Terms and Conditions (https://onlinelibrary.wiley.com/terms-and-conditions) on Wiley Online Library for rules of use; OA articles are governed by the applicable Creative Commons License